Maximal Wavelet Filter and Its Application to Bidecadal Oscillation over the Northern Hemisphere through the Twentieth Century

SHOSHIRO MINOBE

Division of Earth and Planetary Sciences, Graduate School of Science, Hokkaido University, Sapporo, and Frontier Research System for Global Change, Yokohama, Japan

TERUKO MANABE* AND AKIKO SHOUJI

Japan Meteorological Agency, Tokyo, Japan

(Manuscript received 18 May 2001, in final form 26 September 2001)

ABSTRACT

Based on a wavelet transform, a new method referred to as maximal wavelet filter (MWF) is proposed to extract temporal structure changes of a climatic oscillation, which varies its pattern corresponding to the changes of the oscillation period. The MWF is a bandpass filter having a narrow pass band, the central frequency of which temporally varies according to the periods of maximal wavelet amplitudes for a specific region.

MWF is applied to wintertime sea level pressures (SLPs) in the Northern Hemisphere from 1899 to 2000 to extract SLP changes associated with the bidecadal oscillation (BDO), which distributes globally but has the strongest amplitudes in the North Pacific. In the Pacific sector, the BDO center of action captured by the MWF was located over Alaska in the first few decades of the record, and then moved southward to the central North Pacific from 1920 to 1950, with maximal BDO amplitudes in the middle of the century. The southward migration was accompanied by the previously reported increase of the oscillation period from 15 to 20 years. On the other hand, Atlantic SLP variations coherent with the Pacific BDO had large amplitudes in midlatitudes (high latitudes) in the early (late) part of the twentieth century. In association with these spatial structure changes, the pattern of the recent BDO resembles the pattern of the Arctic Oscillation.

The analysis of the sea surface temperatures (SSTs) gridded from the Comprehensive Ocean–Atmosphere Data Set (COADS) and the newly digitized Kobe collections suggests that BDO pattern in the SSTs also shifted toward the south between the first and last few decades of the twentieth century. Furthermore, covariability between the land–air temperatures and Aleutian low strength is observed through the twentieth century for Alaska, but only after 1940 for the midlatitudes of western North America and Hawaii, indicating that the BDO influence was limited to the high latitudes in the first few decades of the twentieth century in these regions, consistent with the spatial structure changes in the SLP field over the North Pacific.

1. Introduction

Recent studies have revealed that one of the most prominent features of earth's climate variability on decadal to centennial timescales is the bidecadal oscillation (BDO; Mann and Park 1994, 1996; White et al. 1997; White and Cayan 1998). The BDO is globally distributed, but has the largest amplitude in the central North Pacific in association with the variability of the Aleutian low (e.g., Mann and Park 1996; White and Cayan 1998). The BDO over the North Pacific has been analyzed from various aspects. Royer (1989) first reported the evidence for the BDO from the analysis of air and water temperatures in Alaska. Subsurface water temperature, mixed layer depth, and Kuroshio transport were reported to exhibit coherent bidecadal oscillations in association with the BDO in the Aleutian lows (Lagerloef 1995; Polovina et al. 1995; Tourre et al. 1999, 2001; Deser et al. 1999). The BDO signatures were captured in the basin-scale or global analyses of surface temperatures (STs) and sea level pressures (SLPs; Ghil and Vautard 1991; Kawamura 1994; Polovina et al. 1995; Mann and Park 1994, 1996; White et al. 1997; White and Cayan 1998; Zhang et al. 1998; Tourre et al. 1999, 2001; Chao et al. 2000; Venegas and Mysak 2000). Most of these studies showed similar spatial patterns in SSTs or SLPs over the North Pacific, but it is still not clear whether the BDO arises from a single physical mechanism or two or more mechanisms. The evidence of the interdecadal variability on about a 20-

* Current affiliation: World Meteorological Organization, Geneva, Switzerland.

Corresponding author address: Dr. Shoshiro Minobe, Division of Earth and Planetary Sciences, Graduate School of Science, Hokkaido University, Sapporo 060-0810, Japan.
E-mail: minobe@ep.sci.hokudai.ac.jp

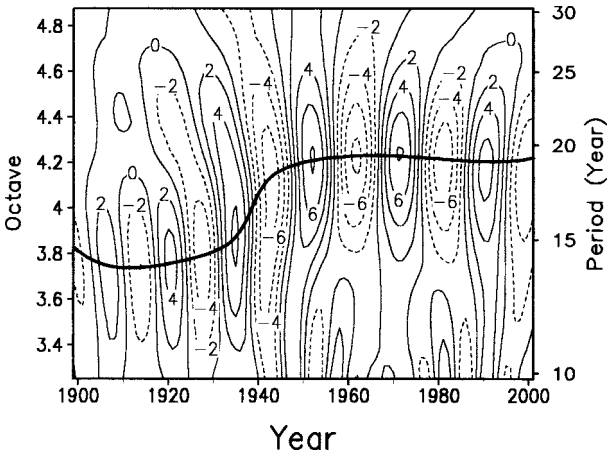

FIG. 1. Wavelet coefficients for the wintertime NPI, which is a SLP time series averaged over 30°–65°N, 160°E–140°W. Contours indicate the real part of the wavelet coeffiecients in units of hPa $yr^{-1/2}$. The thick curve traces the maximal absolute wavelet coefficients between 10- and 30-yr periods.

yr timescale was also observed in tree ring records over North America (Ware 1995; Ware and Thomson 2000; Biondi et al. 2001).

An interesting feature of the BDO in the Pacific sector is that the amplitude and period have changed through the twentieth century; the period was shorter and the amplitude was weaker in the early twentieth century, but in the mid- and late twentieth century, the period was longer and the amplitude was stronger (Fig. 1; details of the figure are explained later). Such changes were first pointed out by Royer (1989) by a regional analysis for Alaska. Minobe (1999, 2000) showed that the period is about 15 yr in the beginning of the twentieth century and that it increased to 20 yr from 1930 to 1950, during which time the BDO amplitude also increased, analyzing basin-scale variations in the atmosphere and the ocean over the North Pacific. A question arises at this point. Has the BDO had a constant spatial pattern regardless of the changes in period through the twentieth century? In order to address this question, we propose here a new methodology, which is referred to as maximal-wavelet filter (MWF). The MWF is a bandpass filter having a narrow-pass band, whose central frequency temporally varies consistent with the periods of maximal wavelet amplitudes for a specific region as explained in detail later.

The rest of the present paper is organized as follows: in section 2, the methodology of the MWF is described, and the data used in the present study is shown in section 3. In section 4, the results of the MWF applied to SLPs in the Northern Hemisphere are shown, and the major MWF results are further examined with respect to their reliability by different techniques. In section 5, we analyze the SST and land surface air temperature (LAT) fields over and around the North Pacific, in order to know whether BDO signatures in these fields varied or not in a consistent manner with the BDO changes in the SLPs. Summary and discussion will be presented in section 6.

2. Maximal wavelet filter

The MWF is closely related to a wavelet transform, and hence we briefly summarize here the main points of the wavelet transform. More complete descriptions of the wavelet transform and various climate research applications of wavelet analysis can be found in Weng and Lau (1994), Lau and Weng (1995), and Torrence and Compo (1998). Temporal wavelet transform coefficient for three-dimensional data are defined as follows:

$$\tilde{f}(x, y, t', a) = W[f(x, y, t)] = \frac{1}{a^{1/2}} \int_{-\infty}^{\infty} f(x, y, t)\psi^*\left(\frac{t - t'}{a}\right) dt, \quad (1)$$

where f is the observed data, $\tilde{f}$ is the wavelet transform coefficient, W is the operator of the wavelet transform, x and y are the zonal and meridional coordinates, respectively, t is the time in units of years, t' is the translation parameter corresponding to the position of the wavelet, a is the scale dilation parameter that determines the width of the wavelet, and ψ^* is the complex conjugate of a mother wavelet, ψ. For the mother wavelet, we employ the Morlet wavelet, which is a commonly used complex mother wavelet and is given by a sinusoidal function modulated by a Gaussian envelope, as the following form:

$$\psi(t) = e^{i\omega_0 t} \exp(-t^2/2), \quad (2)$$

where ω_0 is a constant that defines the width of the Gaussian envelope of the mother wavelet, and is chosen to be 6 in the present study.

The idea of the MWF is based on the fact that the wavelet transform divided by $a^{1/2}$ forms a bandpass filter for each of a. This is clearly seen in the wavelet transform of a sinusoidal time series at an angular frequency, ω, given by

$$\mathrm{Re}\{W[\cos(\omega t)]\} = \sqrt{\frac{\pi a}{2}} e^{-(\omega_0 - \omega a)^2/2} \cos\omega t'. \quad (3)$$

This equation indicates that, for a specific a, a wavelet bandpass filter with the maximal gain of unity at $\omega = \omega_0/a$ can be defined by

$$\sqrt{\frac{2}{\pi a}} W[f]|_a = \sqrt{\frac{2}{\pi}} \frac{1}{a} \int_{-\infty}^{\infty} f(x, y, t)\psi^*\left(\frac{t - t'}{a}\right) dt. \quad (4)$$

The specific a in (4) determines the frequency of the maximal gain, and hence if a varies temporally, we can obtain a filter whose character changes in time. In order to retain substantial energy of an interesting phenomenon in such filtering, a reasonable way to determine the scale dilation parameters is to trace maximal ab-

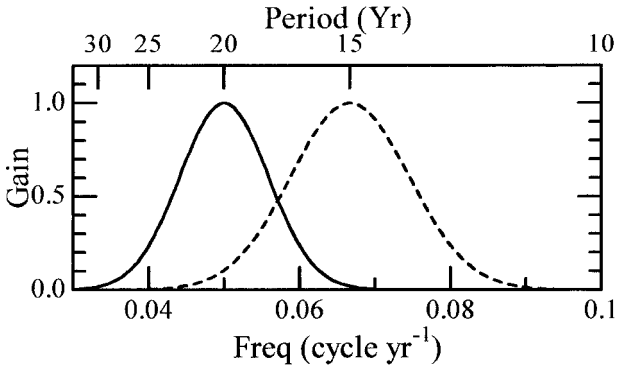

FIG. 2. Gain functions of the MWF for the central frequencies corresponding to a 20-yr (solid curve) and 15-yr period (dashed curve).

solute wavelet amplitudes divided by $a^{1/2}$. Here, the data are multivariate, and hence the absolute wavelet amplitudes to be traced can be obtained by averaging the absolute wavelet amplitudes at each grid point over a specific area, which is chosen so that the energy over the area is dominated by the interesting phenomenon on timescales to be examined. That is, we define $a_{\max}(t')$ as the scale dilation parameters that satisfy

$$\frac{\overline{f}[t', a_{\max}(t')]}{\sqrt{a_{\max}(t')}} > \frac{\overline{f}[t', a_{\max}(t') \pm \varepsilon]}{\sqrt{a_{\max}(t') \pm \varepsilon}}, \tag{5}$$

where $\overline{f}$ is the area-averaged absolute amplitudes of the wavelet transform coefficients, and ε is the arbitrary small number. Consequently, we define MWF as follows:

$$\hat{f}(x, y, t') = \sqrt{\frac{2}{\pi a_{\max}(t')}} W[f]|_{a=a_{\max}(t')} = \sqrt{\frac{2}{\pi}} \frac{1}{a_{\max}(t')} \int_{-\infty}^{\infty} f(x, y, t) \psi^* \left[\frac{t - t'}{a_{\max}(t')}\right] dt, \tag{6}$$

where $\hat{f}$ is the filtered data of complex values. The gain of the MWF is given by $\exp\{-[\omega_0 - \omega a_{\max}(t')]^2\}$, which indicates a narrow peak of a Gaussian form on the frequency domain as illustrated in Fig. 2. In the case where phase delays over the area for averaging are negligible, $\overline{f}$ can be the absolute values of the wavelet transform coefficients of area-averaged time series. This procedure is employed in the application of the present paper as explained in the next section. One can use other mother wavelets rather than the Morlet wavelet for MWF, but it is noteworthy that the mother wavelet should be complex, so that $a_{\max}$ can be detected continuously as a function of time.

In practice, it may be convenient to determine $a_{\max}$ directly from the absolute value of the wavelet transform coefficients (instead of the absolute value divided by $a^{1/2}$), since they are usually examined and plotted. If we define the scale dilation parameter at the maximal wavelet amplitudes as $a'_{\max}$, which satisfies

$$\overline{f}[t', a'_{\max}(t')] > \overline{f}[t', a'_{\max}(t') \pm \varepsilon], \tag{7}$$

$a_{\max}$ is estimated from $a'_{\max}$ as follows:

$$a_{\max}(t') = a'_{\max}(t') \frac{2\omega_0}{\omega_0 + \sqrt{\omega_0^2 + 2}}. \tag{8}$$

It is noteworthy that the filtered data, $\hat{f}$, involves two timescales; one is the oscillation timescale at the period of $2\pi a_{\max}/\omega_0$ [$\approx 1.05\, a_{\max}$, for the present ω_0 (=6)], and the other is the timescale of the slow modulation of the oscillation. In order to focus on the slow modulation, we have found that it is useful to calculate filter data that have relative phases with respect to a representative grid point, x_0, y_0, as follows:

$$\hat{f}_r(x, y, t') = \hat{f}(x, y, t') \frac{\hat{f}(x_0, y_0, t')^*}{|\hat{f}(x_0, y_0, t')|}, \tag{9}$$

where $\hat{f}_r$ has the identical absolute amplitudes to $\hat{f}$, but has relative phases with respect to the representative grid point. We refer to $\hat{f}$ defined by (6) as MWF data, and to $\hat{f}_r$ given by (9) as relative MWF data, respectively.

As with any method for data analysis, the MWF can have some problems. In particular, there are two major sources that may cause artificial results in the MWF; one is low temporal resolution, and the other is the end effects of the record.

The sharp filter gain structure of the MWF shown in Fig. 2 is inevitably accompanied by a low temporal resolution, and can make the temporal changes of spatial structures obtained by the MWF smoother than that which occurs in reality. Thus, when an interesting smooth temporal change is found in the results of the MWF, it is recommended that the results be checked with a conventional bandpass filter that has a wider pass band and hence higher temporal resolution. For this purpose, we will employ a bandpass filter with the half-power points at 10- and 30-yr periods in the following application.

The end effects generally weaken the filtered amplitudes near the beginning and end of a data record. In order to reduce the end effects, before making the wavelet transform, we extend the observed time series by 30% at the beginning and end, using an autoregressive model of an order of 30% of the data length that is fitted by the maximum entropy method (MEM). Without the MEM extension, the MWF for a sinusoidal time series with a 20-yr period recovers more than 70% (90%) of amplitude inside of 12 (25) yr apart from the beginning and end of the records. Reflecting the smaller temporal resolution noted above, the end effects for the MWF are heavier than those for a conventional bandpass filter with a wider pass band; that is, the 10–30-yr bandpass filter recovers more than 90% of amplitude inside of 10 yr apart from the ends. The MEM extension cannot totally remove the end effects. Thus, when the maximal

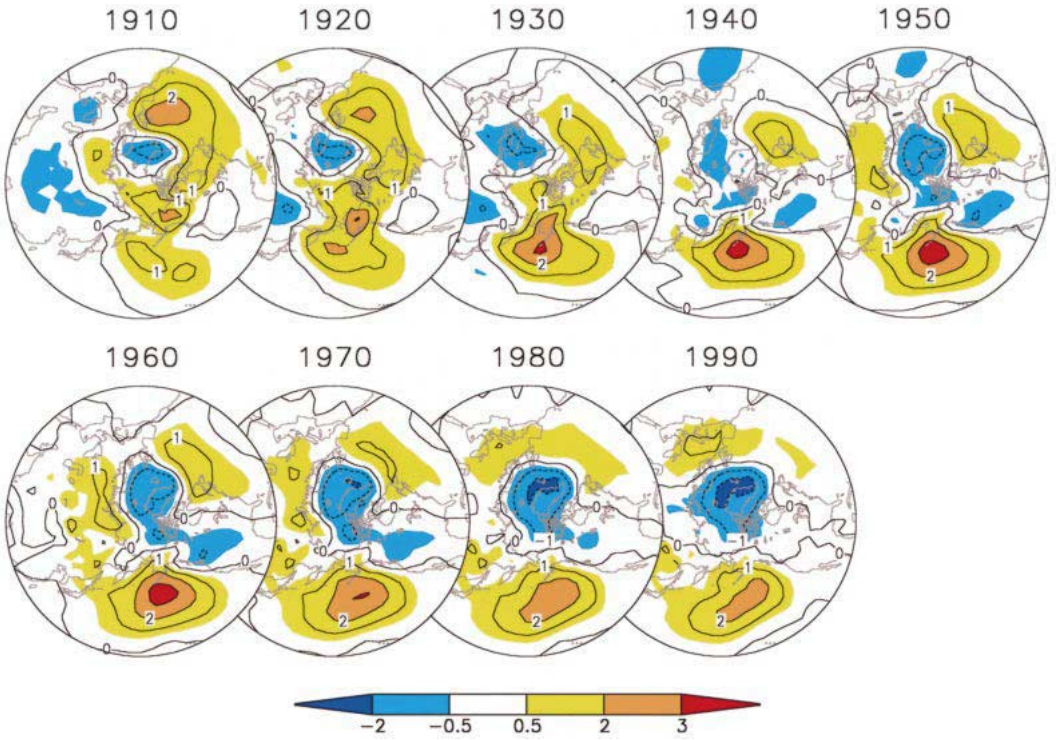

FIG. 3. Real part of the wintertime relative MWF SLPs with respect to 50°N, 165°W from 1910 to 1980 at a 10-yr interval. Contour interval is 1 hPa. Systematic changes in the BDO pattern are seen in the North Pacific and North Atlantic.

amplitudes are found in the middle of the record, we need to carefully address whether the maximum is a realistic feature or an artifact.

3. Data

Wintertime (December–February) SLP data north of 20°N are analyzed by the MWF. The SLP dataset used here is an updated version of the SLP dataset of Trenberth and Paolino (1980), and has monthly mean 5° × 5° grids from January 1899 to July 2000. In the present analysis, we traced $a_{\max}(t')$ for the absolute wavelet amplitudes of the wintertime North Pacific index (NPI), which is an area-averaged SLP time series over 30°–65°N, 160°E–140°W (Trenberth and Hurrell 1994), since the BDO observed in the NPI is known to exhibit an interesting phase modulation as shown in Fig. 1 (see also Minobe 1999, 2000). The thick curve in Fig. 1 is $a'_{\max}$, from which we can estimate $a_{\max}$ using (8). Then, MWF given by (6) is applied to the wintertime SLPs over the Northern Hemisphere. The SLP data between 20° and 70°N are available at most of the grid points throughout the century, but the data in higher latitudes (75°, 85°, and 90°N) are missing in the early part of the record. When an unavailable datum is sandwiched by available data both at the northern and southern grid points, the datum is filled with the mean value of the northern and southern data. For the unavailable data that cannot be filled by this meridional interpolation, EOFs for seasonal anomalies are used for filling the data values. The data at 75°N before 1940 are mainly filled by the meridional interpolation, while the data at 85°N (90°N) before 1946 (1940) are filled by the EOF interpolation. Except for these high latitudes, the interpolations do not influence the major results of the present paper.

A gridded SST dataset is produced from observations contained in the newly digitized Kobe collection, available before 1933, together with the observations in the Comprehensive Ocean–Atmosphere Data Set (COADS; Woodruff et al. 1987). The features of the newly digitized Kobe collection are described by Manabe (1999). By adding the Kobe collection, the number of available ship reports are increased significantly, and especially reached about 100 000 reports during World War I against about 20 000 reports stored in the COADS. Quality control of the data are applied based on the monthly climatology and standard deviations on a monthly 2° × 2° grid box using the data from 1960 to 1990. Observations that have a larger difference than 3.5 times the standard deviation from the climatology are not used for gridding. The observations that passed the quality control criterion within the monthly 2° × 2° grid box are averaged to form monthly mean SSTs on the grid box. Then, the monthly anomalies are calculated based on the gridded monthly mean SST data, and the

monthly anomalies are further averaged spatially and seasonally to produce SST anomalies on a 4° × 10° grid in latitude and longitude during the cold season (November–May) in order to obtain a relatively better coverage of the gridded data.

We also analyze wintertime land surface air temperature (LAT) data around the North Pacific. The monthly 5° × 5° gridded LAT data from January 1880 to June 1999 is the gridded version of the Global Historical Climate Network (GHCN; Vose et al. 1992), and the gridding method was described by Baker et al. (1995).

The use of the winter SLP and LAT data and cold season SSTs is consistent with the seasonality of the BDO signature shown by Minobe (2000); the BDO signature in the SLP field was only found in the winter season, but the BDO in the SST field is observed not only in the winter season but also in the spring (March–May) season with weaker amplitudes probably due to the lagged response of the ocean.

4. SLP

Figure 3 shows the real part of wintertime relative MWF SLPs with respect to 50°N, 165°W from 1910 to 1980 at a 10-yr sampling interval. In the Pacific sector, strong amplitudes were confined over Alaska in 1910. As time progresses from 1920 to 1950, the Pacific action center moves into the central North Pacific. The BDO amplitude takes its maximum around 1950 with an oval pattern. After 1950, the amplitudes weaken slightly, and the oscillation pattern elongates in a southwest–northeastward direction. In the Atlantic sector, the BDO signature appears as a meridional dipole pattern similar to the North Atlantic Oscillation (NAO). However, the contribution from the midlatitudes was strong in the early twentieth century, whereas in the late twentieth century the amplitudes are larger in the Arctic region. Near the end of the twentieth century, the enhanced arctic amplitudes make the overall pattern resemble the Arctic Oscillation proposed by Thompson and Wallace (1998). Consequently, the BDO center of action has migrated from the high to midlatitudes in the North Pacific, but in contrast, the region of the larger contribution changes from mid- to high latitudes in the North Atlantic.

The MWF SLPs are complex valued data similar to complex EOFs, and hence we can examine phase propagation by using the MWF data. Interesting phase propagation is observed in the MWF SLPs over the North Pacific from 1930 to the present, as exemplified for the data in 1960 in Fig. 4. The phases exhibit continuous increase from the Pacific Northwest to the Kamchatka Peninsula across the amplitude maxima in the central North Pacific, with phase differences of about 90°. The validity of the phase propagation is examined by calculating coherency and phase spectra of SLPs between 45°N, 140°W and 60°N, 180° using a method described by Hannan (1970) and von Storch and Zwiers (1999).

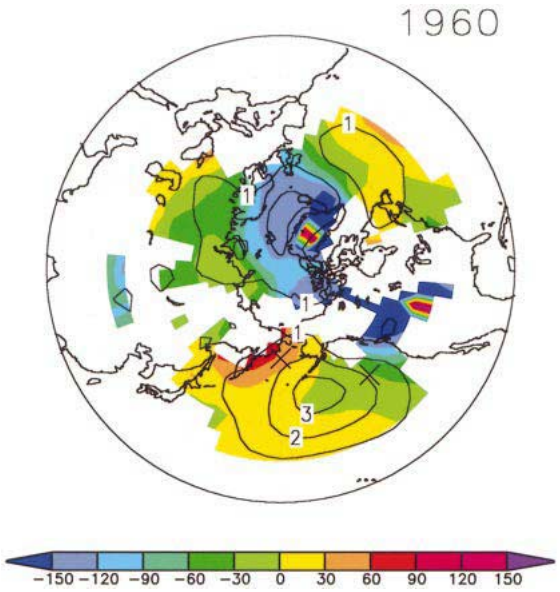

FIG. 4. Absolute amplitudes (contour) and phases (color) of the relative MWF SLPs with respect to 50°N, 165°W, in year 1960. The contour interval is 1 hPa, and the phases are colored for the region where the amplitudes are greater than 0.5 hPa. The direction of increasing phase is the direction of propagation. The X's indicate locations of 45°N, 140°W and 60°N, 180°, and the phase spectra between them indicate a statistically significant phase delay (see text).

The resultant coherency exhibits a bidecadal peak, and the phase spectrum at the peak is significantly different from 0° and from 180° at the 90% confidence limit, suggesting that the propagation is physically meaningful. The propagation feature in the North Pacific on the bidecadal timescale is also seen in a multitaper method–singular value decomposition (MTM–SVD) analysis of SLP and Atlantic sea ice by Venegas and Mysak (2000, their Fig. 14), though a MTM–SVD analysis of SLP and SST by Tourre et al. (2001) showed an almost opposite direction of SLP propagation. The discrepancy of the propagation direction may be due to the different seasons analyzed; we have analyzed winter SLP data, but Tourre et al. (2001) analyzed the year-round SLPs.

The reliability of the BDO pattern changes that are captured by the MWF is examined using EOFs for the SLPs as follows. First, we separate the 102 yr (1899–2000) of wintertime SLP data into three 34-yr segments (1899–1932, 1933–66, 1967–2000), and the 10–30-yr bandpass filter is independently applied to each data segment. The 30-yr cutoff period is used in order to avoid the energy leakage from an oscillation with a 50–70-yr period (e.g., Minobe 1997, 1999, 2000). Thus, end effects of the filtering are expected to influence three data segments equally. EOFs are calculated for each of the three filtered SLP data segments over the North Pacific region (30°–70°N, 120°E–80°W), and regression coefficients between the PC-1 (first principle component) and SLPs over the Northern Hemisphere are obtained (Fig. 5). In the first epoch (1899–1932), the BDO

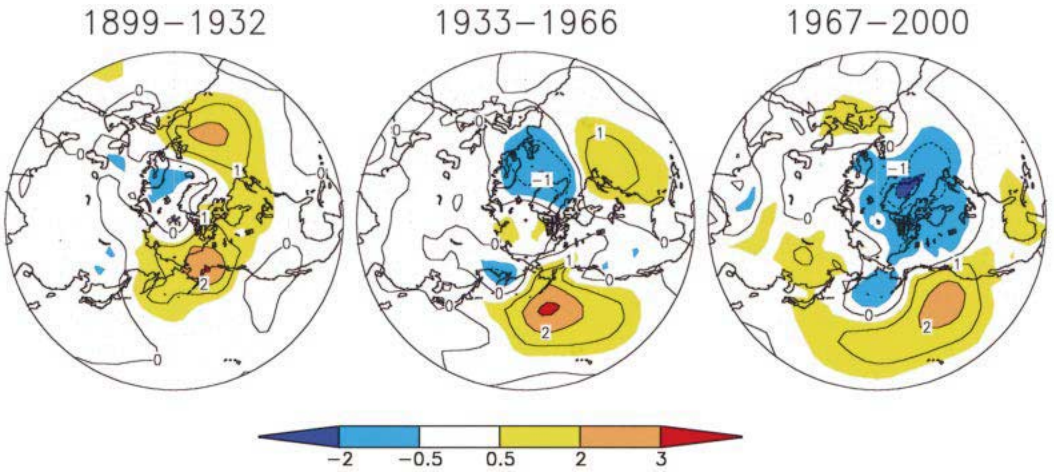

FIG. 5. Regression maps of the SLPs onto the PC-1s for the 10–30-yr bandpass-filtered SLP data for the data segments from (left) 1899–1932, (middle) 1933–66, and (right) 1967–2000. The EOFs are calculated for the North Pacific, 30°–70°N, 120°E–80°W. Contour and color conventions are the same as those used in Fig. 3.

variability occurred over Alaska, but in the second epoch (1933–66), the signal is found in the central North Pacific. In the last epoch (1967–2000), the maximal amplitude is slightly reduced and the pattern is elongated in the northeastern and southwestern direction. In the Atlantic sector, the negative regressions in high latitudes and positive regressions in midlatitudes are common in the three regression maps, but amplitudes in high latitudes (midlatitudes) are stronger in the last (first) epoch, with roughly similar amplitudes between the high and midlatitudes in the second epoch. These features obtained by EOF analysis are consistent with the results of the MWF described above.

The southward move of the BDO center of action captured in the MWF SLPs in the Pacific sector is now more closely examined in a latitude–time section (Fig. 6a). The MWF SLPs indicate that significant amplitudes are confined north of 60°N in the first few decades, and that they then move toward the south from 1920 to 1950 with the center of the variability at about 45°N in 1950. From 1950 to the present, the amplitude maxima stayed at approximately the same latitude. In order to know whether or not the continuous southward migration is an artifact associated with the low temporal resolution of the MWF as noted above, we also examine SLPs with the 10–30-yr bandpass filter (Fig. 6b). As shown in the appendix, the 10–30-yr bandpass filter is expected to be able to distinguish between a continuous migration and a sudden shift of an activity center. Qualitatively the same features are evident in the 10–30-yr bandpass-

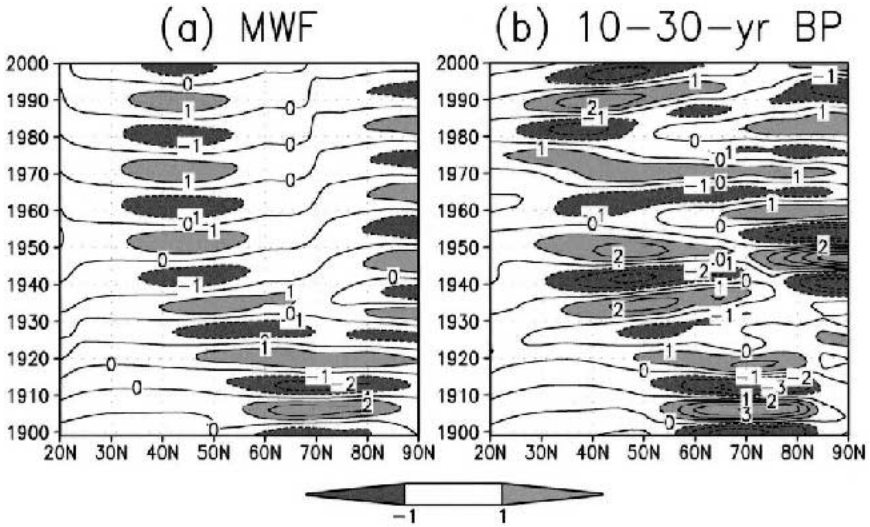

FIG. 6. Latitude–time cross section averaged over 160°E–120°W (a) for the MWF SLPs and (b) for the 10–30-yr bandpass-filtered SLPs. Contour interval is 1 hPa. Both data exhibited southward migration of the BDO from 1920 to 1950.

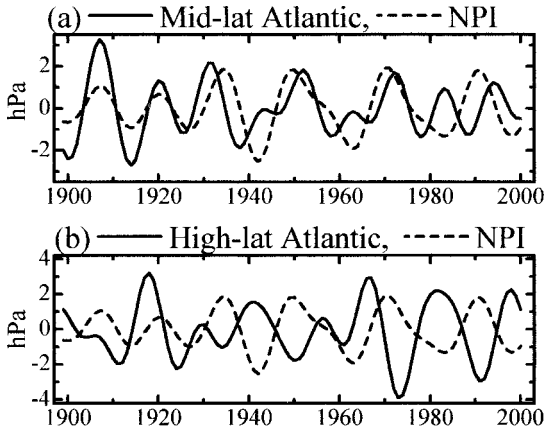

FIG. 7. Bandpass filtered (10 yr < period < 30 yr) SLPs (solid curves) (a) over the midlatitude Atlantic (40°–55°N, 60°W–0°) and (b) over the high-latitude Atlantic (60°–75°N, 60°W–0°), along with the filtered NPI (dashed curves).

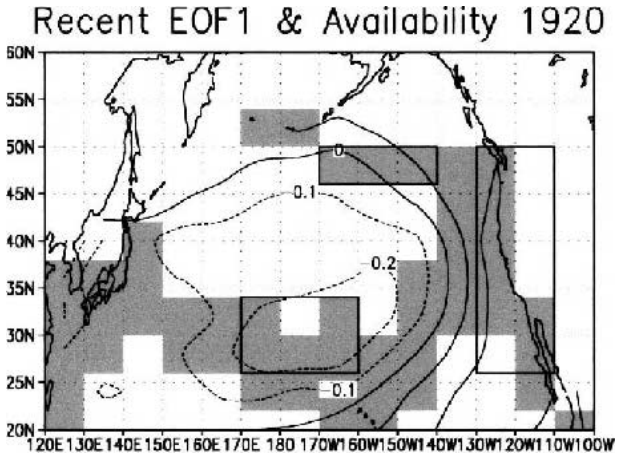

FIG. 8. The first EOF for the cold season (Nov–May) SST from 1950 to 1995 (contours) and continuously available data grids from 1920 to 1995 (shaded). Rectangles show the regions where SST data are averaged and resultant SST time series are closely examined (see text).

filtered SLPs, suggesting that the continuous southward migration of the BDO center of action from 1920 to 1950 occurred in reality.

The 10–30-yr bandpass-filtered SLPs are also examined in order to know whether or not the filtered data are consistent with the changes of the BDO structure in the Atlantic sector observed by the MWF. As described above, the MWF showed that the NAO-like BDO in Atlantic SLPs had large amplitudes in mid- (high) latitudes in the early (late) twentieth century. We examine two area-averaged SLP time series; one is averaged over 40°–55°N, 60°W–0° (midlatitudes) and the other over 60°–75°N, 60°W–0° (high latitudes). These two average areas coincide with the regions of large variances for the raw and 10–30-yr filtered winter SLP data in the Atlantic sector, and the SLP difference between them gives an index for the NAO. As expected, the NAO index (NAOI) defined here has a high correlation with Hurrell's (1995) winter (December–March) NAOI, which is defined as the normalized SLP difference between Lisbon, Portugal, and Stykkisholmur/Reykjavik, Iceland; the correlation coefficient is 0.88 (0.68) with (without) the 10–30-yr bandpass filter. The 10–30-yr filtered midlatitude SLP time series had an in-phase relation with the NPI until 1970 and its amplitude continuously decreased through the record (Fig. 7). On the other hand, the high-latitude SLP time series has been out-of-phase with the NPI after 1940 with relatively large amplitude after 1960s. This result confirms that the dominant BDO contributions in the North Atlantic occurred in the midlatitudes in the early twentieth century, but in high latitudes near the end of the twentieth century, as shown by the MWF.

5. SST and LAT

It is interesting to examine whether physical parameters of the atmosphere and ocean other than SLP support the century-scale changes of the BDO spatial structure observed in SLPs over the North Pacific. The first parameter to be examined is SST, since the SLP structure changes mainly occurred over the ocean. Unfortunately, the coverage of the SST data is relatively poor in the early twentieth century as shown in Fig. 8. Thus, we must carefully choose regions where SSTs are examined from the point of view of the coverage of available data and the physical meaning of the data. In order to know which regions are physically meaningful, we calculated the first EOF of the 10–30-yr bandpass-filtered cold season SST after 1950, during which available SST data have almost complete coverage in the North Pacific. Consistent with previous studies of the SST changes of the BDO (e.g., Mann and Park 1996; White and Cayan 1998), the first EOF exhibits oval-shaped anomalies in the central North Pacific accompanied by horseshoe-shaped anomalies with the opposing polarity to the east and to the north of the oval (Fig. 8). If the pattern of the bidecadal SST variation changed in association with the migration of the BDO center of action in the SLPs, then the most prominent changes may have occurred around the boundary between the oval and horseshoe regions in the central-northern North Pacific. In this physically interesting region, the data from 46°–50°N to 170°–140°W have better availability. Thus, we have chosen to focus on the SST data over this region (referred to as boundary SST). Also, for a comparison, we examine two other area-averaged SST time series over 26°–34°N, 170°E–160°W (referred to as oval SST) and 26°–50°N, 130°–110°W (horseshoe SST). These regions are shown in Fig. 8 by rectangles.

Figure 9 shows the 10–30-yr bandpass-filtered time series of the boundary SST along with the oval and horseshoe SSTs. The oval and horseshoe SSTs are out of phase throughout the record, indicating that the over-

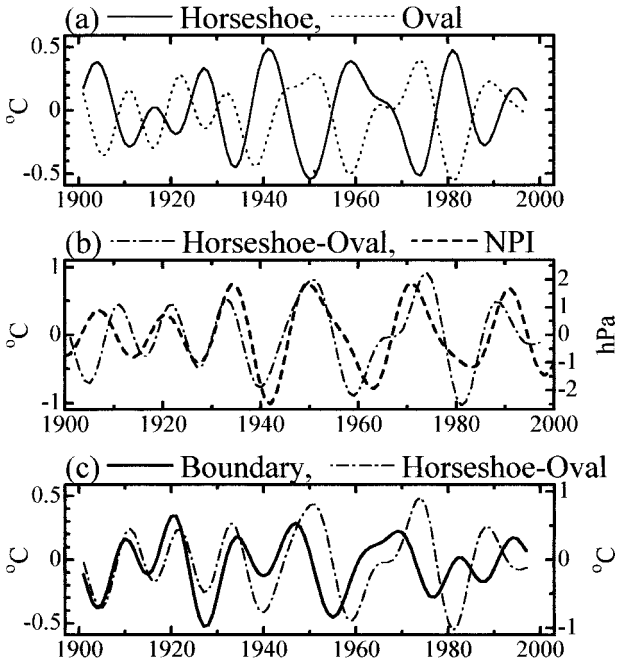

FIG. 9. (a) Cold season SST time series averaged over 26°–50°N, 130°–110°W (thin solid curve, denoted as horseshoe), and over 26°–34°N, 170°E–160°W (thin dashed curve, denoted as oval). (b) Cold season horseshoe-minus-oval SST (thin dash–dotted curve) and winter NPI (thick dashed curve, right-hand axis). (c) Cold season SST time series averaged over 46°–50°N, 170°–140°W (thick black curve, denoted as boundary) and horseshoe-minus-oval SST (thin dash-dotted curve, right-hand axis). All time series are filtered by the 10–30-yr bandpass filter.

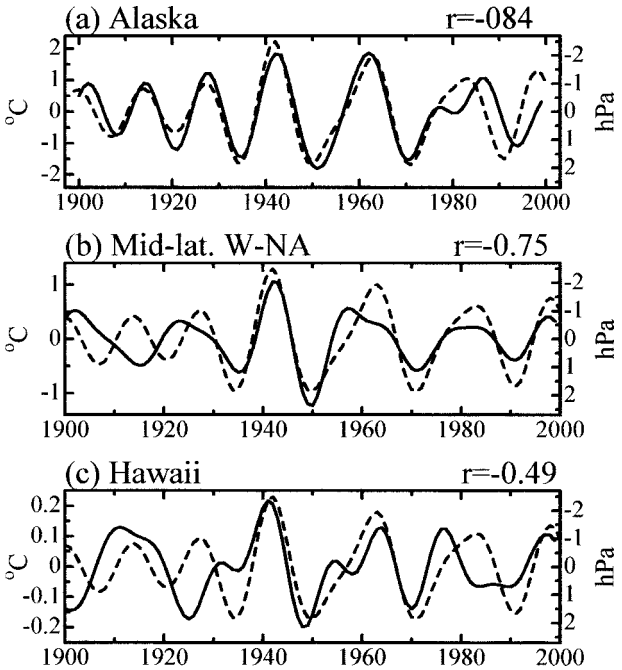

FIG. 10. Bandpass-filtered (10 yr < period < 30 yr) LATs (solid curves) over (a) Alaska (55°–65°N, 180°–140°W), (b) midlatitude western North America (30°–55°N, 140°–105°W) and (c) Hawaii (20°–25°N, 160°–155°W), along with the NPI (dashed curves) in each panel. For an easier comparison, the axis for the NPI on the right-hand side is reversed (negative direction is toward the top of the page). The numbers at the top-right corner of each panel indicates the correlation coefficients between the LATs and NPIs.

all seesaw relation between them is unchanged throughout the twentieth century. The temporal changes of the seesaw oscillations are coherent with the bidecadal changes of the NPI except during the first 10 years. The boundary SST was in-phase (out of phase) with the oval (horseshoe) SST in the early twentieth century, but these phase relationships have reversed since 1980. Consequently, the oval (horseshoe) SST dominates the boundary region in the first (last) few decades, and hence the boundary between the oval and horseshoe SSTs in the first few decades is likely to be located to the north of the present location. In other words, the nodal line between the oval and horseshoe SSTs shifted toward the south between the first and last few decades in the twentieth century. This result is consistent with the southward migration of the BDO observed in the SLP field.

The structure changes of the BDO are also examined by analyzing LAT data around the North Pacific. Figure 10 shows the 10–30-yr bandpass-filtered time series of wintertime LAT over Alaska (55°–65°N, 180°–140°W), midlatitude western North America (30–55°N, 140–105°W), and Hawaii (20°–25°N, 160°–155°W). Signatures of the BDO were detected in the first 2 air temperature time series by a wavelet analysis (Minobe 2000). All time series are out-of-phase with the NPI after 1940 (notice that NPIs are reversed in Fig. 10), but only the Alaska data hold the relationship throughout the twentieth century; for midlatitude North America and Hawaii, coherent changes of the LATs with the NPI are absent before 1930. This result again suggests that the BDO Pacific sector variability prevailed mainly in the high latitudes during the first few decades of the twentieth century.

6. Conclusions and discussion

In order to extract the spatial changes of an interesting oscillatory phenomenon corresponding to the changes of its period, a new data analysis method, the maximal wavelet filter (MWF), has been proposed. The MWF is a bandpass filter with a narrow pass band of a Gaussian form, and the frequency for the maximal gain temporally varies by tracing the periods of maximal wavelet amplitudes for a specific region. The calculation of the MWF consists of two steps. First, the maximal absolute amplitudes of the wavelet coefficients divided by the root of the scale dilation parameter are traced for a specific region, and corresponding scale dilation parameters, $a_{\max}$, are determined as a function of time. Second, the temporally varying filter defined by (6) for $a_{\max}$ is applied to global data. In order to focus on the slow modulation

of the oscillation, it is convenient to examine MWF data relative to a specific location as given by (9).

The MWF captures century-scale changes of the BDO in the wintertime SLP field over the North Pacific and North Atlantic. The MWF SLPs indicates there was a southward migration of the BDO center of action in the twentieth century over the North Pacific; the center of action located over Alaska in the early twentieth century, and changed its position to the central North Pacific from 1920 to 1950. In the Atlantic sector, the BDO contribution shifted from the midlatitudes to the high latitudes between the beginning and end of the century. These features are confirmed by an EOF analysis for the three 34-yr segments of the SLPs with the 10–30-yr bandpass filter. The continuous migration in the Pacific sector seen in the MWF SLPs is also observed in the 10–30-yr bandpass-filtered SLPs, which have higher temporal resolution than the MWF. The BDO structure obtained by the MWF shares the major features found by the previous analyses, especially for the energetic wintertime Aleutian low changes (see Mann and Park 1996; White and Cayan 1998; Tourre et al. 1999). However, the previous studies assumed a constant spatial structure of the BDO, and ignored the interesting spatial structure changes of the BDO that were important before 1950.

We also examined the SST and LAT fields. The gridded SST data are produced from COADS and the newly digitized Kobe collection. The SST analysis strongly suggests that the boundary between the oval and horseshoe SSTs shifted toward the south between the few early and late decades of the twentieth century. The LAT analysis has indicated that the high-latitude BDO in the LAT field continued through the twentieth century but its penetration into the midlatitudes around the North Pacific was limited after 1940. These SST and LAT results are generally consistent with the southward migration of the BDO center of action in the SLP field in the Pacific sector.

From the aspect of the methodology, the present results have shown that the MWF is a useful tool for analyzing temporal changes of spatial structures corresponding to frequency changes. This is demonstrated by the fact that scale dilation parameters for the maximal wavelet amplitudes are continuously detected as a function of time. On the other hand, if scale dilation parameters at the maximal wavelet amplitudes are discontinuous for a record period, MWF may not give physically meaningful information throughout the period. However, it is not difficult to determine whether scale dilation parameters at the maximal wavelet amplitudes are continuous or not when one calculates the wavelet transform for a representative time series. Because wavelet transform is rapidly getting popular in climate studies, the authors propose the MWF as a helpful tool for studying spatial changes of the oscillatory signals. MWF should be used with care; MWF can have problems near the beginning and end of a record as with other filtering methods, and MWF generally has coarser temporal resolution than conventional bandpass filters that have a wider pass band. These disadvantages can be overcome by using EOFs and conventional bandpass filter complementarily as described in the present paper. Consequently, if one uses MWF for a proper problem with enough care, MWF should help significantly.

The spatial structure changes of the BDO have substantial implications on the mechanism of the BDO. Several papers proposed that the BDO arises from the air–sea interaction in the Pacific Ocean (Latif and Barnett 1994, 1996; Gu and Philander 1997; Jin 1997; White and Cayan 1998; Knutson and Manabe 1998; Weng and Neelin 1999; Talley 1999; Yukimoto et al. 2000; Cessi 2000; Gallego and Cessi 2000). It is noteworthy that all of the mechanisms considered in these papers are more or less a delay-negative feedback mechanism, though the physical processes for the delay can be different. In a delay-negative feedback model, the oscillation period is generally proportional to the delay time, and hence a wider ocean basin, which can involve a longer delay time, may be related with a longer oscillation period. In the early twentieth century, the bidecadal oscillation had a shorter timescale with midlatitude contribution from the North Atlantic, whereas after the middle of the twentieth century the midlatitude contribution was observed in the Pacific basin with a longer BDO timescale. Thus, the authors would like to point out the possibility that change of the spatial structure and timescale of the BDO may be related to changes of the relative contributions between the Pacific and Atlantic Oceans. The observed BDO might arise from a combination of multiple modes in these oceans with the possibility of vigorous interactions. This hypothesis is, of course, at a crude speculative stage, but would be worth examining with air–sea coupled models in future.

Another interesting implication of the spatial structure changes of the BDO concerns climatic regime shifts over the North Pacific. It is known that the North Pacific experienced prominent regime shifts in the 1920s, 1940s, and 1970s, represented by strength changes of Aleutian lows (e.g., Kondo 1988; Hare and Francis 1995; Dettinger and Cayan 1995; Zhang et al. 1997; Minobe 1997; Mantua et al. 1997). A climatic regime shift is defined as a transition from one climatic state to another within a period substantially shorter than the lengths of the individual epochs of each climate state (e.g., Minobe 1997). In particular, the shift in the 1970s has attracted much attention in the last decade, and a number of analyses showed a series of dramatic changes of the physical environment (e.g., Nitta and Yamada 1989; Trenberth 1990; Graham 1994; Tanimoto et al. 1993; Trenberth and Hurrell 1994; Miller et al. 1994, 1998; Polovina et al. 1995, Lagerloef 1995, Yasuda and Hanawa 1997; Nakamura et al. 1997; Zhang and Levitus 1997; Schneider et al. 1999; Tourre et al. 1999; Zhang and Liu 1999; Suga et al. 2000; Hare and Mantua 2000).

Minobe (1999, 2000) proposed that the three climatic regime shifts resulted from the quasi-simultaneous phase reversals of the BDO and a 50–70-yr oscillation [referred to as Pacific Pentadecadal oscillation (PPO)] with comparable amplitudes, and that the superposition of the BDO and PPO gives the Pacific (inter)decadal Oscillation (PDO). The PDO was proposed by Mantua et al. (1997), and a recent review for a wide range of studies for the PDO is given by Mantua and Hare (2002). The BDO and PPO are considered essentially different phenomena because of their different seasonality in SLP and LAT fields (Minobe 1999, 2000) and because of their different spatial structures in SST fields (Chao et al. 2000). The above interpretation suggests that the changes in the characteristics of the BDO over the North Pacific can cause important changes in climatic regime shifts and the PDO. For example, a phase reversal of the PPO around 1890 identified from spring air temperatures over midlatitude western North America by Minobe (1997) may not have been accompanied by an *abrupt* strength change of the Aleutian low. This may be because the BDO may have mainly prevailed in high latitudes in the late nineteenth century, as well as observed in the beginning of the twentieth century in the present results. A similar lack of prominent regime shifts due to a lack of the simultaneous phase reversals between the BDO and PPO were observed in the spring NPI time series in the 1940s and 1970s (Minobe 1999, 2000). Consequently, in order to understand the nature of the regime shifts and the PDO, we need to carefully examine the behavior of both the BDO and PPO in models and in observed data, without expecting that the BDO has a fixed spatial structure.

Acknowledgments. We thank A. Gershunov, N. Mantua, and the editor, F. Zwiers, for their insightful and constructive comments for the original version of this paper; P. Cessi for invaluable discussion; W. B. White, N. Schneider, R.-H. Zhang, Y. Tourre, L. Talley, and R. E. Thomson for preprints and reprints; and J. Hurrell for the NAO time series. Some figures are produced with the GrADS package developed by B. Doty. This study is supported by grants from the Japanese Ministry of Education, Culture and Science, and a fund from Core Research for Evolution Science and Technology (CREST), Japan Science and Technology Corporation (JST).

APPENDIX

A Test for MWF and a Bandpass Filter

In order to know how the MWF and a bandpass filter having a wider pass band treat abrupt changes in the spatial and temporal characters of oscillations, the following test data are examined by these filters. The test data are given by

$$u(y, t) = \begin{cases} \exp\{-[(y - y_1)/w]^2\} \sin[(t - t_0)2\pi/p_1], & 0 < t < t_0 \\ \exp\{-[(y - y_2)/w]^2\} \sin[(t - t_0)2\pi/p_2], & t_0 < t < T, \end{cases} \quad \text{(A1)}$$

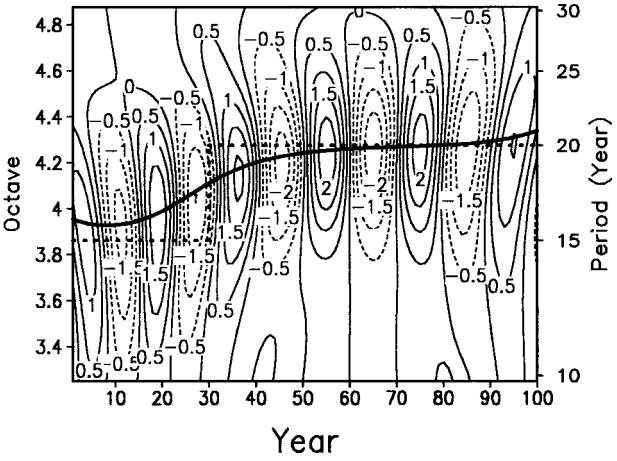

FIG. A1. Same as Fig. 1, but for the test data given by (A1). The dotted line indicates the scale dilation parameters corresponding to the true oscillation periods.

where t is the time, T is the length of the record, y is the distance. The variations of the data are temporally sinusoidal, and spatially Gaussian with an e-folding scale of w, but the location of the action center (y_1, y_2) and periods (p_1, p_2) abruptly change at the time of t_0. We set T as 100, t_0 as 30, y_1 as 70, y_2 as 45, p_1 as 15, p_2 as 20, and w as 20, aiming to imitate some features of the observed SLP changes in the Pacific sector shown in Fig. 6. Figure A1 shows that the trace of $a'_{\max}$ (and hence the trace of $a_{\max}$ also) does not correctly capture the given abrupt change of the oscillation period as expected. Furthermore, the $y - t$ diagram shown in Fig. A2a exhibits that it is difficult to confidentially conclude whether the spatial structure change is a continuous migration or a discontinuous position shift from the MWF data. The 10–30-yr period bandpass-filtered data, however, more strongly suggest that it is a discontinuous shift (Fig. A2b). Thus, when a smooth temporal change of spatial structures is observed by the MWF, it is recommended to examine the observed data using a bandpass filter that has a wider pass band than the MWF.

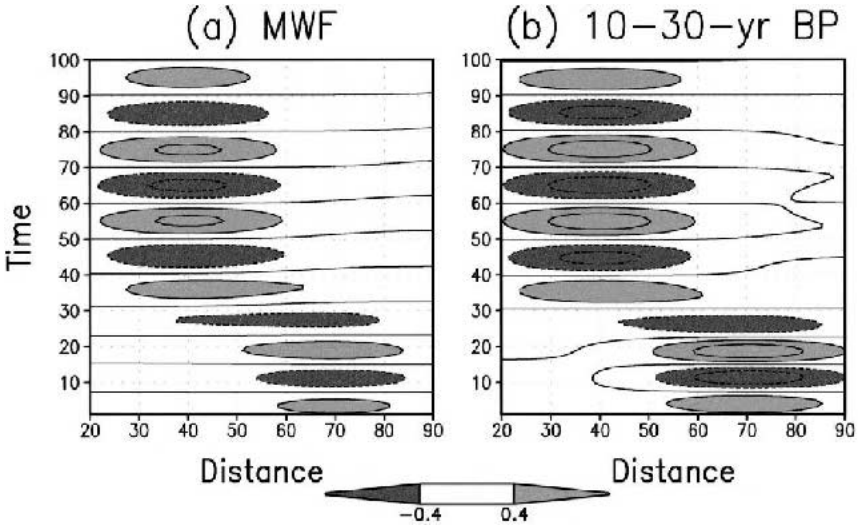

FIG. A2. Same as Fig. 6, but for the test data given by (A1). The given abrupt shift of the location of the oscillation is more prominent in the 10–30-yr bandpass-filtered data (right) than in the MWF data.

REFERENCES

Baker, C. B., J. K. Eischeid, T. R. Karl, and H. F. Diaz, 1995: The quality control of long-term climatological data using objective data analysis. Preprints, *Ninth Conf. on Applied Climatology*, Dallas, TX, Amer. Meteor. Soc., 15–20.

Biondi, F., A. Gershunov, and D. R. Cayan, 2001: North Pacific decadal climate variability since 1661. *J. Climate,* **14,** 5–10.

Cessi, P., 2000: Thermal feedback on wind stress as a contributing cause of climate variability. *J. Climate,* **13,** 232–244.

Chao, Y., M. Ghil, and J. C. McWilliams, 2000: Pacific interdecadal variability in this century's sea surface temperatures. *Geophys. Res. Lett.*, **27,** 2361–2364.

Deser, C., M. A. Alexander, and M. S. Timlin, 1999: Evidence for a wind-driven intensification of the Kuroshio Current extension from the 1970s to the 1980s. *J. Climate,* **12,** 1697–1706.

Dettinger, M. D., and D. R. Cayan, 1995: Large-scale atmospheric forcing of recent trends toward early snowmelt runoff in California. *J. Climate,* **8,** 606–623.

Gallego, B., and P. Cessi, 2000: Exchange of heat and momentum between the atmosphere and the ocean: A minimal model of decadal oscillations. *Climate Dyn.,* **16,** 479–489.

Ghil, M., and R. Vautard, 1991: Interdecadal oscillations and the warming trend in global temperature time series. *Nature,* **350,** 324–327.

Graham, N. E., 1994: Decadal scale variability in the 1970's and 1980's: Observations and model results. *Climate Dyn.,* **10,** 135–162.

Gu, D. F., and S. G. H. Philander, 1997: Interdecadal climate fluctuations that depend on exchanges between the tropics and extratropics. *Science,* **275,** 805–807.

Hannan, E. J., 1970: *Multiple Time Series.* Wiley, 536 pp.

Hare, S. R., and R. C. Francis, 1995: Climate change and salmon production in the Northeast Pacific Ocean. *Can. Spec. Publ. Fish. Aquat. Sci.*, **121,** 357–372.

——, and N. Mantua, 2000: Empirical evidence for North Pacific regime shifts in 1977 and 1989. *Progress in Oceanography,* Vol. 47, Pergamon, 99–103.

Hurrell, J. W., 1995: Decadal trends in the North Atlantic Oscillation: Regional temperatures and precipitation. *Science,* **269,** 676–679.

Jin, F.-F., 1997: A theory of interdecadal climate variability of the North Pacific ocean–atmosphere system. *J. Climate,* **10,** 324–338.

Kawamura, R., 1994: A rotated EOF analysis of global sea surface temperature variability with interannual and interdecadal scales. *J. Phys. Oceanogr.,* **24,** 707–715.

Knutson, T. R., and S. Manabe, 1998: Model assessment of decadal variability and trends in the tropical Pacific Ocean. *J. Climate,* **11,** 2273–2296.

Kondo, J., 1988: Volcanic eruptions, cool summers and famines in the northeastern part of Japan. *J. Climate,* **1,** 775–788.

Lagerloef, G. S. E., 1995: Interdecadal variations in the Alaska gyre. *J. Phys. Oceanogr.,* **25,** 2242–2258.

Latif, M., and T. P. Barnett, 1994: Causes of decadal climate variability over the North Pacific and North America. *Science,* **266,** 634–637.

——, and ——, 1996: Decadal climate variability over the North Pacific and North America: Dynamics and predictability. *J. Climate,* **9,** 2407–2423.

Lau, K.-M., and H. Weng, 1995: Climate signal detection using wavelet transform: How to make a time series sing. *Bull. Amer. Meteor. Soc.,* **76,** 2391–2402.

Manabe, T., 1999: The digitized Kobe Collection, Phase I: Historical surface marine meteorological observations in the archive of the Japan Meteorological Agency. *Bull. Amer. Meteor. Soc.,* **80,** 2703–2715.

Mann, M. E., and J. Park, 1994: Global-scale modes of surface temperature variability on interannual to century timescale. *J. Geophys. Res.,* **99** (D12), 25 819–25 833.

——, and ——, 1996: Joint spatiotemporal modes of surface temperature and sea level pressure variability in the Northern Hemisphere during the last century. *J. Climate,* **9,** 2137–2162.

Mantua, N. J., and S. R. Hare, 2002: The Pacific decadal oscillation. *J. Oceanogr.,* **58,** 35–44.

——, ——, Y. Zhang, J. M. Wallace, and R. C. Francis, 1997: A Pacific interdecadal climate oscillation with impacts on salmon production. *Bull. Amer. Meteor. Soc.,* **78,** 1069–1079.

Miller, A. J., D. R. Cayan, T. P. Barnett, N. E. Graham, and J. M. Oberhuber, 1994: The 1976–77 climate shift of the Pacific Ocean. *Oceanography,* **7,** 21–26.

——, ——, and W. B. White, 1998: A westward-intensified decadal change in the North Pacific thermocline and gyre-scale circulation. *J. Climate,* **11,** 3112–3127.

Minobe, S., 1997: A 50–70 year climatic oscillation over the North Pacific and North America. *Geophys. Res. Lett.,* **24,** 683–686.

——, 1999: Resonance in bidecadal and pentadecadal climate oscil-

lations over the North Pacific: Role in climatic regime shifts. *Geophys. Res. Lett.,* **26,** 855–858.
——, 2000: Spatio-temporal structure of the pentadecadal variability over the North Pacific. *Progress in Oceanography,* Vol. 47, Pergamon, 99–102.
Nakamura, H., G. Lin, and T. Yamagata, 1997: Decadal climate variability in the North Pacific during the recent decades. *Bull. Amer. Meteor. Soc.,* **98,** 2215–2225.
Nitta, T., and S. Yamada, 1989: Recent warming of tropical sea surface temperature and its relationship to the Northern Hemisphere circulation. *J. Meteor. Soc. Japan,* **67,** 375–383.
Polovina, J. J., G. T. Mitchum, and G. T. Evans, 1995: Decadal and basin-scale variation in mixed layer depth and the impact on biological production in the central and North Pacific, 1960–88. *Deep-Sea Res.,* **42,** 1701–1716.
Royer, T. C., 1989: Upper ocean temperature variability in the northeast Pacific: Is it an indicator of global warming? *J. Geophys. Res.,* **94** (C12), 18 175–18 183.
Schneider, N., A. J. Miller, M. A. Alexander, and C. Deser, 1999: Subduction of decadal North Pacific temperature anomalies: Observations and dynamics. *J. Phys. Oceanogr.,* **29,** 1056–1070.
Suga, T., A. Kato, and K. Hanawa, 1999: North Pacific Tropical Water: Its climatology and temporal changes associated with regime shift in the 1970s. *Progress in Oceanography,* Vol. 47, Pergamon, 223–256.
Talley, L. D., 1999: Simple coupled midlatitude climate models. *J. Phys. Oceanogr.,* **29,** 2016–2037.
Tanimoto, Y., N. Iwasaka, K. Hanawa, and Y. Toba, 1993: Characteristic variation of sea surface temperature with multiple time scales in the North Pacific. *J. Climate,* **6,** 1153–1160.
Thompson, D. W. J., and J. M. Wallace, 1998: The Arctic Oscillation signature in the wintertime geopotential height and temperature fields. *Geophys. Res. Lett.,* **25,** 1297–1300.
Torrence, C., and G. P. Compo, 1998: A practical guide to wavelet analysis. *Bull. Amer. Meteor. Soc.,* **79,** 61–78.
Tourre, Y. M., Y. Kushnir, and W. B. White, 1999: Evolution of interdecadal variability in sea level pressure, sea surface temperature, and upper ocean temperature over the Pacific Ocean. *J. Phys. Oceanogr.,* **29,** 1528–1541.
——, B. Rajagopalan, Y. Kushnir, M. Barlow, and W. B. White, 2001: Patterns of coherent decadal and interdecadal climate signals in the Pacific basin during the 20th century. *Geophys. Res. Lett.,* **28,** 2069–2072.
Trenberth, K. E., 1990: Recent observed interdecadal climate changes in the Northern Hemisphere. *Bull. Amer. Meteor. Soc.,* **71,** 988–993.
——, and D. A. Paolino, 1980: The Northern Hemisphere sea-level pressure data set: Trends, errors, and discontinuities. *Mon. Wea. Rev.,* **108,** 855–872.
——, and J. W. Hurrell, 1994: Decadal atmosphere–ocean variations in the Pacific. *Climate Dyn.,* **9,** 303–319.
Venegas, S. A., and L. A. Mysak, 2000: Is there a dominant timescale of natural climate variability in the Arctic? *J. Climate,* **13,** 3412–3434.
von Storch, H., and F. W. Zwiers, 1999: *Statistical Analysis in Climate Research.* Cambridge University Press, 483 pp.
Vose, R. S., R. L. Schmoyer, P. M. Steurer, T. C. Peterson, R. Heim, T. R. Karl, and J. Eischeid, 1992: The Global Historical Climatology Network: Long-term monthly temperature, precipitation, sea level pressure, and station pressure data. Carbon Dioxide Information Analysis Center, Oak Ridge National Laboratory ORNL/CDIAC-53, NDP-041, 315 pp.
Ware, D. M., 1995: A century and a half of change in the climate of the NE Pacific. *Fish. Oceanogr.,* **4,** 267–277.
——, and R. E. Thomson, 2000: Interannual and multidecadal timescale climate variations in the northeast Pacific. *J. Climate,* **13,** 3209–3220.
Weng, H., and K.-M. Lau, 1994: Wavelets, period doubling, and time-frequency localization with application to organization of convection over the tropical western Pacific. *J. Atmos. Sci.,* **51,** 2523–2541.
Weng, W., and J. D. Neelin, 1999: Analytical prototypes for ocean–atmosphere interaction at midlatitude. Part II: Mechanisms for coupled gyre modes. *J. Climate,* **12,** 2757–2774.
White, W. B., and D. R. Cayan, 1998: Quasi-periodicity and global symmetries in interdecadal upper ocean temperature variability. *J. Geophys. Res.,* **103** (C10), 21 335–21 354.
——, J. Lean, D. R. Cayan, and M. D. Dettinger, 1997: Response of global upper ocean temperature to changing solar irradiance. *J. Geophys. Res.,* **102** (C2), 3255–3266.
Woodruff, S. D., R. J. Slutz, R. L. Jenne, and P. M. Steurer, 1987: A Comprehensive Ocean–Atmosphere Data Set. *Bull. Amer. Meteor. Soc.,* **68,** 1239–1250.
Yasuda, T., and K. Hanawa, 1997: Decadal changes in the mode waters in the midlatitude North Pacific. *J. Phys. Oceanogr,* **27,** 858–870.
Yukimoto, S., M. Endoh, Y. Kitamura, A. Kitoh, T. Motoi, and A. Noda, 2000: Two distinct interdecadal modes of the Pacific Ocean and atmospheric variability with a coupled GCM. *J. Geophys. Res.,* **105,** 13 945–13 963.
Zhang, R.-H., and S. Levitus, 1997: Structure and cycle of decadal variability of upper ocean temperature in the North Pacific. *J. Climate,* **10,** 710–727.
——, and Z. Liu, 1999: Decadal thermocline variability in the North Pacific Ocean: Two pathways around the subtropical gyre. *J. Climate,* **12,** 3273–3296.
Zhang, X., J. Sheng, and A. Shabbar, 1998: Modes of interannual and interdecadal variability of Pacific SST. *J. Climate,* **11,** 2556–2569.
Zhang, Y., J. M. Wallace, and D. S. Battisti, 1997: ENSO-like interdecadal variability: 1900–1993. *J. Climate,* **10,** 1004–1020.